Role of locally polar regions in the superconductivity of SrTiO₃

Salva Salmani-Rezaie ◉, Hanbyeol Jeong ◉, Ryan Russell ◉, John W. Harter ◉, and Susanne Stemmer ◉*
Department of Materials, University of California, Santa Barbara, Santa Barbara, California 93106-5050, USA

Understanding the interaction between polar and superconducting order parameters may hold the key to several classes of superconductors that remain poorly understood, including SrTiO₃ and several tellurides. Here we show that doped, strained SrTiO₃ films can exhibit both global or local polar order, respectively, depending on the amount of epitaxial mismatch strain, thereby providing a platform to understand how inversion symmetry breaking affects superconductivity. We find that the superconducting critical temperature correlates with the length scale of polar order. In particular, the transition temperature is enhanced when polar nanodomains are sufficiently large or, in the extreme limit, films are globally ferroelectric. In these cases, the Cooper pairs reside in a noncentrosymmetric environment. Conversely, low transition temperatures are found when the nanodomains are small. The findings point to the length scale of polar nanodomains and spin-orbit coupling as important parameters controlling the superconductivity of SrTiO₃. The ability to control the size of the polar domains opens up new opportunities to design and control the nature of superconductivity in a wide range of materials.

I. INTRODUCTION

Superconductivity in SrTiO₃ cannot be described by conventional electron-phonon models and its Cooper pairing mechanism remains a subject of significant debate, just like that of many other unconventional superconductors [1]. Recently, suggestions that superconductivity in SrTiO₃ is associated with the proximity to ferroelectric order have gained significant interest [2–12]. Although pure and unstrained SrTiO₃ is not believed to be ferroelectric [13], ferroelectricity can be induced in doped samples that subsequently become superconducting, for example, by ¹⁸O isotope substitution, alloying, or strain [14–18]. Ferroelectric materials are also noncentrosymmetric, which means that spin-orbit coupling can become an important energy scale [19,20]. Spin-orbit coupling can give rise to unconventional superconducting states, including mixed parity and topological superconductivity, and unusual magnetoelectric and magnetochiral effects [5,9,10,19–23]. In addition, ferroelectric samples exhibit an enhancement of the superconducting transition temperature (T_c) by up to a factor of 2 [15–18], which has not yet been explained with any of the current theories.

We have recently shown that polar nanodomains are present far above the ferroelectric transition temperature and that they are an essential precursor of the ferroelectric state [24,25]. Their size decreases with increasing carrier density until eventually the ferroelectric transition is suppressed [24]. Small polar nanodomains exist even in unstrained SrTiO₃, which does not become ferroelectric [24–27]. The role of *local* inversion symmetry breaking in the superconductivity of SrTiO₃ has not yet been considered. Moreover, polar nanodomains have also been discovered in the parent phases

of other classes of superconductors, such as the tellurides [28–30], hinting at a connection to superconductivity that is more general than is currently appreciated. One reason for the lack of understanding is the low superconducting transition temperatures, which make it difficult to characterize symmetry breakings at the nanoscale with existing tools. The behavior of the nanodomains is, however, systematic as a function of carrier density, strain, and with distance from the ferroelectric transition [24,25]; therefore reliable extrapolations can be made even from room temperature observations.

The goal of the present study is to investigate the potential role of the polar (nano)domains in determining the superconducting transition temperature (T_c). To this end we keep the carrier density constant but vary the degree of strain relaxation in epitaxial thin films of SrTiO₃, which will be shown to affect the ferroelectric transition. We observe an enhancement of superconductivity in samples with correlated polar distortions regardless of the emergence of ferroelectricity. Our results point to inversion symmetry breaking as the main parameter controlling superconductivity in SrTiO₃.

II. EXPERIMENTAL

Doped SrTiO₃ films were grown on (001) (LaAlO₃)₀.₃(Sr₂TaAlO₆)₀.₇ (LSAT) single crystals by hybrid molecular beam epitaxy (MBE), as described elsewhere [17,31]. For coherently strained films, the LSAT substrates impose a 1% in-plane compressive strain. Near the peak of the superconducting dome, the T_c of coherently strained films exceeds 600 mK, which is at least twice that of unstrained films [32]. We use the rare earth ions Sm (films A and C) and La (films B and D) as dopants. As shown previously, T_c does not depend on the type of dopant [32]. Electrical measurements between 300 and 2 K were performed in a Quantum Design Dynacool system. The carrier density (n_{3D})

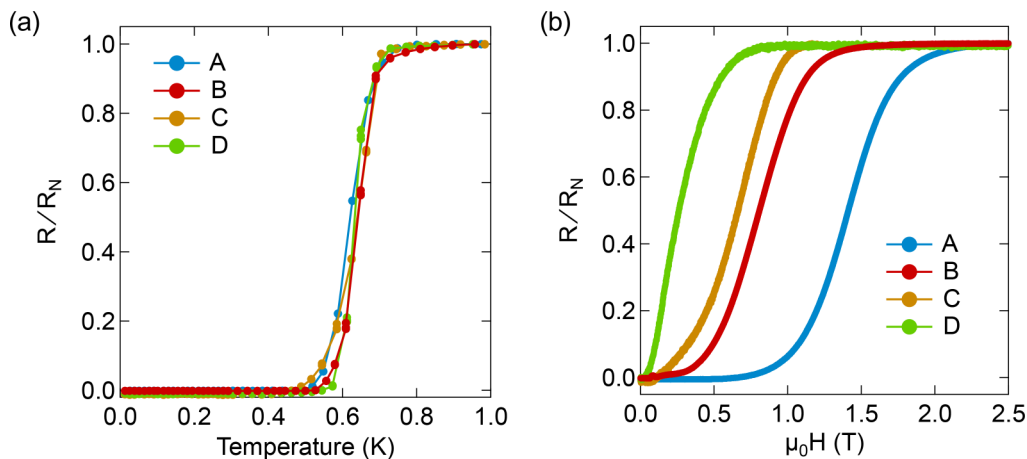*Corresponding author: stemmer@mrl.ucsb.edu

FIG. 1. Normalized resistance (R/R_N) as a function of (a) temperature and (b) out-of-plane magnetic field for films A–D at 50 mK.

was calculated from the Hall effect at 300 K and ranged between 6 and 8×10^{19} cm^{-3}, which is slightly underdoped. Measurements below 1 K were carried out in an Oxford Instruments Triton dilution refrigerator. Cryofilters at the mixing chamber of the dilution refrigerator were used to decrease effective electron temperature [33]. The films' resistance was measured using lock-in amplifiers at low frequency (11 Hz). T_c was defined as the temperature at which the resistance, R, was 5% of the normal-state resistance, R_N. The superconducting upper critical field (H_{c2}) was defined as the value of the magnetic field ($\mu_0 H$) when R reaches 95% of R_N. The superconducting coherence length was estimated as $\xi_0 = \sqrt{\phi_0/2\pi H_{C2}}$, where ϕ_0 is the magnetic flux quantum.

A high-resolution Philips Panalytical X'pert thin-film x-ray diffractometer with Cu Kα radiation was used to quantify the degree of strain relaxation. The thickness of the films was $\sim$180 nm, which is near the critical thickness for strain relaxation on LSAT [34]. Sample A was fully strained (see Fig. S1 in the Supplemental Material [35]), while films B, C, and D all showed some strain relaxation, as seen by a slight shift of the out-of-plane lattice parameter from its fully strained value and the absence of thickness fringes (see Fig. S1 [35]). Optical second harmonic generation (SHG) experiments were performed using an ultrafast laser supplying 40-fs pulses at a 10-kHz repetition rate and a center wavelength of 800 nm. The laser spot size was 30 μm, and the fluence was below 10 mJ/cm^2. SHG signals were normalized to the incident laser beam power. Cross-section transmission electron microscopy (TEM) samples were prepared using a FEI Helios Dualbeam NanoLab 600 focused ion beam for atomic-resolution scanning transmission electron microscopy (STEM). High-angle annular dark-field (HAADF) images were obtained using Thermo-Scientific Talos G2 200$\times$ S/TEM (Cs = 1.2 mm) at 200 keV with a semiconvergence angle of 10.5 mrad. Twenty fast scan images (2048 $\times$ 2048 pixels, 2 μs dwell time) were sequentially recorded and cross-correlated to enhance the signal-to-noise ratio and minimize scan distortion. Position-averaged convergent beam diffraction (PACBED) patterns [36] were obtained for all analyzed images to ensure that the sample tilt is less than 1 mrad. Atomic column positions can be determined with picometer precision [25,37]. Here, the off-centering of Ti-O columns from the positions in a cubic,

centrosymmetric cell are used as a measure of the unit-cell polarization, as described elsewhere [25]. The polarization direction is defined based on the difference between the center of mass of the four neighboring Sr columns and the Ti-O column position. All images were obtained at room temperature.

III. RESULTS

Figure 1(a) shows normalized resistances (R/R_N) as a function of temperature. The extracted T_c values are similar and correspond to 600, 600, 560, and 580 mK for samples A–D, respectively. All T_c values are enhanced relative to unstrained SrTiO$_3$ and in line with those previously reported for coherently strained SrTiO$_3$ [17], despite the fact that samples B–D are partially strain-relaxed. Minor variations in T_c are expected, similar to previous observations, and can be due to small variations in the carrier density [32]. Figure 1(b) shows the normalized resistances as a function of the magnetic field at 50 mK. Unlike T_c, H_{c2} varies between the samples. Table I summarizes the sample parameters.

Figure 2 shows temperature-dependent SHG intensity for samples A–D between 200 and 10 K. Upon cooling, only the fully strained sample A shows a sharp increase in the SHG response, which indicates the transition to a globally ferroelectric phase at $\sim$90 K. As shown previously, the electric polarization is normal to the film plane in film A [18]. In contrast, samples B, C, and D do not show a ferroelectric transition. The SHG signal changes gradually with temperature, excluding the possibility of any long-range ordered ferroelectric polarization, whether in plane or out of plane, with a length scale greater than the laser wavelength. In particular, the presence of ferroelectric domains larger than the laser

TABLE I. Superconducting and materials parameters of films A–D.

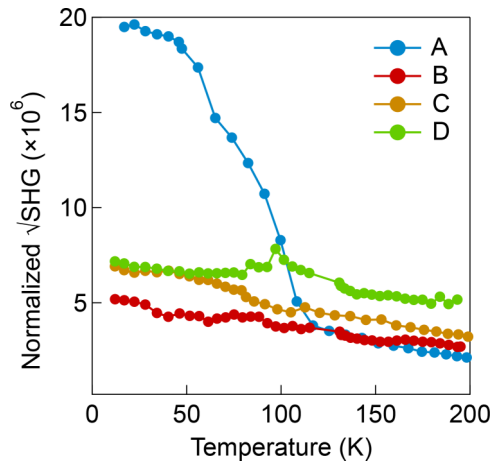| Sample	Dopant	n_{3D}(cm^{-3})	T_c (mK)	H_{c2} (T)	ξ (nm)
A	Sm	6×10^{19}	600	1.75	13.7
B	La	8×10^{19}	600	1.22	16.4
C	Sm	8×10^{19}	550	0.98	18.3
D	La	7×10^{19}	580	0.63	22.8

FIG. 2. Temperature dependence of the SHG intensity of films A–D. Only film A shows a sharp transition from a paraelectric to a ferroelectric phase.

wavelength but smaller than the laser spot size would give rise to a speckle pattern that is not observed experimentally. Instead, in all the samples a weak but finite SHG signal persists to high temperatures, which is likely due to a combination of diffuse SHG from the presence of polar nanodomains [24,25], smaller than the laser wavelength, and higher-order optical processes such as electric quadrupole SHG that do not depend on the breaking of inversion symmetry.

Figure 3 shows the results from the analysis of HAADF-STEM images that provide information about polar nan-

odomains in the fully strained and partially relaxed $SrTiO_3$ films, respectively. The HAADF-STEM images can be found in Fig. S2 [35]. The displacements of the Ti-O columns in each unit cell are color coded, with the color indicating the $\langle 001 \rangle$ direction closest to the direction of the polarization vector. In film A the Ti-O columns displace primarily along [001] (red color) and form large polar nanodomains. The other films (B–D) have smaller domains with polarizations parallel to $[00\bar{1}]$, [010], and $[0\bar{1}0]$, respectively. The larger nanodomains are on order of eight unit cells with average Ti-O column displacements of $\sim$10 pm for all films. The polarization direction in the nanodomains in the partially relaxed films does not have a strong preference for the out-of-plane direction, in contrast to film A. The different polarization directions average out to give an isotropic, but finite, SHG signal. Analysis of additional regions can be found in Fig. S3 (Supplemental Material [35]) and give similar results.

IV. DISCUSSION AND CONCLUSIONS

To briefly summarize the results, SHG shows that only the fully strained film A transitions to long-range ferroelectric order. All films show polar nanodomains, even if there is no ferroelectric transition. Nevertheless, all films exhibit a substantially enhanced T_c. Thus a long-range ordered ferroelectric state is not required for enhanced T_c.

The results can be explained if T_c is controlled by the relative length scales of polar domains and the spatial separation of the Cooper pairs. The extreme case is a globally
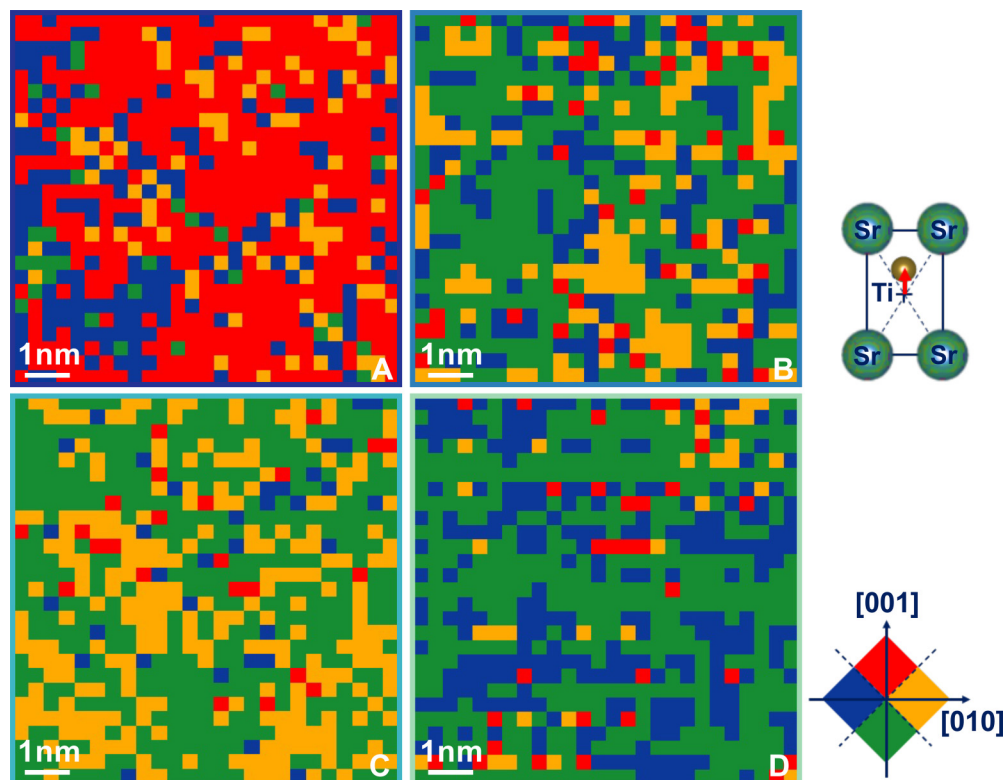

FIG. 3. HAADF-STEM results showing polar domains in films A–D. Each pixel represents the displacement of the Ti-O column in that unit cell. Displacements are color coded based on the proximity of the polarization vector to the nearest $\langle 001 \rangle$ direction.
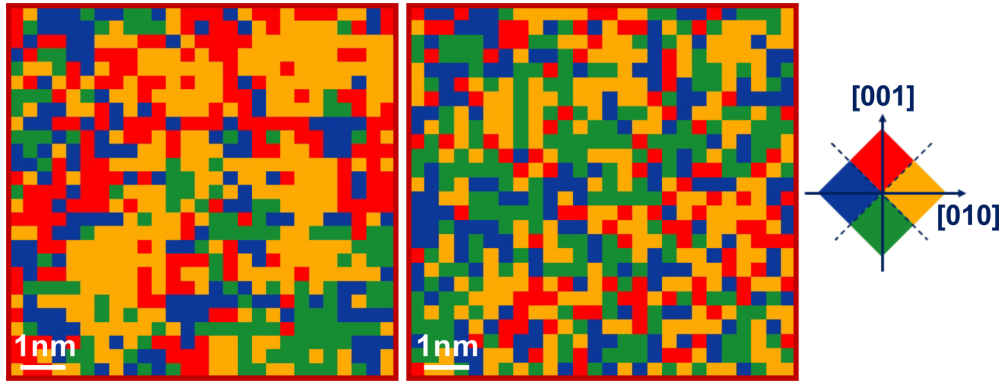
FIG. 4. HAADF-STEM results showing polar domains in (a) unstrained and (b) overdoped strained $SrTiO_3$ film.

ferroelectric film which forms a single domain for compressively strained films [18]. In this picture, sufficiently large nanodomains achieve the same enhancement of T_c as a ferroelectric film as long as the Cooper pair separation is not too large. Importantly, nanodomains will grow in size as the temperature is lowered, as can, for example, be seen by gradual increase of SHG signal with temperature. To test this picture, we next discuss two films whose nanodomains are *small* compared to the Cooper pair separation (Fig. 4). The first case is an unstrained $SrTiO_3$ film grown on an $SrTiO_3$ substrate ($n_{3D} \sim 7 \times 10^{19}$ cm^{-3}), and the second is a fully strained $SrTiO_3$ film on LSAT with a high carrier density in the overdoped regime ($n_{3D} \sim 3 \times 10^{20}$ cm^{-3}). The value of T_c for the unstrained film is 227 mK, while it is 160 mK for the overdoped, strained film (shown previously in Ref. [17]). Both films show T_c values that are in line with expectations at these carrier densities [17], e.g., T_c is *not* enhanced. Nanodomains in the overdoped film were also shown in Ref. [24]. Data shown in Fig. 4 were analyzed to allow for a direct comparison with Fig. 3. As can be seen from Fig. 4, while the unstrained film shows polar nanodomains, they are very small, spanning on average 3.9 ± 0.9 unit cells. No nanodomains exist at room temperature in the overdoped film, although small nanodomains might still form at lower temperatures [24]. T_c is rapidly suppressed upon a slight increase in carrier density, when nanodomains do not form at any temperature due to the screening by the free carriers [17].

Thus all results are consistent with the length scale of polar order determining T_c of $SrTiO_3$. This finding points to a crucial role of inversion symmetry breaking in the superconductivity of $SrTiO_3$, and, in turn, of spin-orbit coupling, which is present only in a noncentrosymmetric material. In particular, if the polar domains are larger than the separation of the Cooper pairs, then the Cooper pairs reside in a polar or noncentrosymmetric material. In contrast, if the polar domains are smaller than the separation between the pairs, they reside in an (on average) centrosymmetric film, which, as has been shown here, results in a low T_c. One could take this picture one step further and suggest that superconductivity in $SrTiO_3$ *requires* inversion symmetry breaking. This would provide a natural explanation as to why ferroelectricity and superconductivity vanish at similar carrier densities on the overdoped side, where the nanodomains collapse upon screening by the free carriers. It would also explain recent observations of a relatively constant but low T_c in the very underdoped regime [38], where the nanodomains are small relative to the separation of the Cooper pairs but never completely vanish [24,26,27].

The importance of local polar regions and their length scale thus point to spin-orbit coupling as the key to Cooper pairing in $SrTiO_3$. Our results are remarkably consistent with findings that showed a strong correlation between the strength of Rashba spin-orbit coupling and T_c in quasi-two-dimensional electron gases in $SrTiO_3$ [39]. The importance of spin-orbit coupling in the superconductivity of $SrTiO_3$ would also explain the surprising insensitivity of T_c to magnetic impurities [32,40].

The results should motivate a microscopic theory of the role of spin-orbit coupling and dipolar interactions in the superconductivity $SrTiO_3$. Finally, as mentioned above, locally polar regions continue to be discovered in the parent phases of many other unconventional superconductors [28–30], while other incipient ferroelectrics have shown unexpected superconductivity [41]. It is therefore possible that Cooper pairing is governed by polar or inversion symmetry broken regions in a much wider range of materials than has previously been appreciated.

[1] M. N. Gastiasoro, J. Ruhman, and R. M. Fernandes, Superconductivity in dilute SrTiO$_3$: A review, Ann. Phys. **417**, 168107 (2020).

[2] J. Appel, Soft-Mode superconductivity in SrTiO$_{3-x}$, Phys. Rev. **180**, 508 (1969).

[3] S. E. Rowley, L. J. Spalek, R. P. Smith, M. P. M. Dean, M. Itoh, J. F. Scott, G. G. Lonzarich, and S. S. Saxena, Ferroelectric quantum criticality, Nat. Phys. **10**, 367 (2014).

[4] J. M. Edge, Y. Kedem, U. Aschauer, N. A. Spaldin, and A. V. Balatsky, Quantum Critical Origin of the Superconducting Dome in SrTiO$_3$, Phys. Rev. Lett. **115**, 247002 (2015).

[5] Y. X. Wang, G. Y. Cho, T. L. Hughes, and E. Fradkin, Topological superconducting phases from inversion symmetry breaking order in spin-orbit-coupled systems, Phys. Rev. B **93**, 134512 (2016).

[6] Y. Kedem, Novel pairing mechanism for superconductivity at a vanishing level of doping driven by critical ferroelectric modes, Phys. Rev. B **98**, 220505(R) (2018).

[7] K. Dunnett, A. Narayan, N. A. Spaldin, and A. V. Balatsky, Strain and ferroelectric soft-mode induced superconductivity in strontium titanate, Phys. Rev. B **97**, 144506 (2018).

[8] D. v. d. Marel, F. Barantani, and C. W. Rischau, Possible mechanism for superconductivity in doped SrTiO$_3$, Phys. Rev. Res. **1**, 013003 (2019).

[9] S. Kanasugi and Y. Yanase, Spin-orbit-coupled ferroelectric superconductivity, Phys. Rev. B **98**, 024521 (2018).

[10] S. Kanasugi and Y. Yanase, Multiorbital ferroelectric superconductivity in doped SrTiO$_3$, Phys. Rev. B **100**, 094504 (2019).

[11] V. Kozii, Z. Bi, and J. Ruhman, Superconductivity Near a Ferroelectric Quantum Critical Point in Ultralow-Density Dirac Materials, Phys. Rev. X **9**, 031046 (2019).

[12] C. Enderlein, J. F. de Oliveira, D. A. Tompsett, E. B. Saitovitch, S. S. Saxena, G. G. Lonzarich, and S. E. Rowley, Superconductivity mediated by polar modes in ferroelectric metals, Nat. Commun. **11**, 4852 (2020).

[13] K. A. Muller and H. Burkard, SrTiO$_3$: An intrinsic quantum paraelectric below 4 K, Phys. Rev. B **19**, 3593 (1979).

[14] C. W. Rischau, X. Lin, C. P. Grams, D. Finck, S. Harms, J. Engelmayer, T. Lorenz, Y. Gallais, B. Fauque, J. Hemberger, and K. Behnia, A ferroelectric quantum phase transition inside the superconducting dome of Sr$_{1-x}$Ca$_x$TiO$_{3-\partial}$, Nat. Phys. **13**, 643 (2017).

[15] C. Herrera, J. Cerbin, K. Dunnett, A. V. Balatsky, and I. Sochnikov, Strain-engineered interaction of quantum polar and superconducting phases, Phys. Rev. Mater. **3**, 124801 (2019).

[16] Y. Tomioka, N. Shirakawa, K. Shibuya, and I. H. Inoue, Enhanced superconductivity close to a non-magnetic quantum critical point in electron-doped strontium titanate, Nat. Commun. **10**, 738 (2019).

[17] K. Ahadi, L. Galletti, Y. Li, S. Salmani-Rezaie, W. Wu, and S. Stemmer, Enhancing superconductivity in SrTiO$_3$ films with strain, Sci. Adv. **5**, eaaw0120 (2019).

[18] R. Russell, N. Ratcliff, K. Ahadi, L. Y. Dong, S. Stemmer, and J. W. Harter, Ferroelectric enhancement of superconductivity in compressively strained SrTiO$_3$ films, Phys. Rev. Mater. **3**, 091401(R) (2019).

[19] M. V. Edel'shtein, Characteristics of the Cooper pairing in two-dimensional noncentrosymmetric electron systems, ZhETF **95**, 2151 (1989) [Sov. Phys. JETP **68**, 1244 (1989)].

[20] M. Sigrist, Introduction to unconventional superconductivity in non- centrosymmetric metals, AIP Conf. Proc. **1162**, 55 (2009).

[21] M. Smidman, M. B. Salamon, H. Q. Yuan, and D. F. Agterberg, Superconductivity and spin–orbit coupling in non-centrosymmetric materials: A review, Rep. Prog. Phys. **80**, 036501 (2017).

[22] V. Kozii and L. Fu, Odd-Parity Superconductivity in the Vicinity of Inversion Symmetry Breaking in Spin-Orbit-Coupled Systems, Phys. Rev. Lett. **115**, 207002 (2015).

[23] R. Wakatsuki, Y. Saito, S. Hoshino, Y. M. Itahashi, T. Ideue, M. Ezawa, Y. Iwasa, and N. Nagaosa, Nonreciprocal charge transport in noncentrosymmetric superconductors, Sci. Adv. **3**, e1602390 (2017).

[24] S. Salmani-Rezaie, K. Ahadi, and S. Stemmer, Polar nanodomains in a ferroelectric superconductor, Nano Lett. **20**, 6542 (2020).

[25] S. Salmani-Rezaie, K. Ahadi, W. M. Strickland, and S. Stemmer, Order-Disorder Ferroelectric Transition of Strained SrTiO$_3$, Phys. Rev. Lett. **125**, 087601 (2020).

[26] K. A. Muller, W. Berlinger, and E. Tosatti, Indication for a novel phase in the quantum paraelectric regime of SrTiO$_3$, Z. Phys. B Condens. Mater. **84**, 277 (1991).

[27] E. K. H. Salje, O. Aktas, M. A. Carpenter, V. V. Laguta, and J. F. Scott, Domains within Domains and Walls within Walls: Evidence for Polar Domains in Cryogenic SrTiO$_3$, Phys. Rev. Lett. **111**, 247603 (2013).

[28] E. S. Bozin, C. D. Malliakas, P. Souvatzis, T. Proffen, N. A. Spaldin, M. G. Kanatzidis, and S. J. L. Billinge, Entropically stabilized local dipole formation in lead chalcogenides, Science **330**, 1660 (2010).

[29] B. Sangiorgio, E. S. Bozin, C. D. Malliakas, M. Fechner, A. Simonov, M. G. Kanatzidis, S. J. L. Billinge, N. A. Spaldin, and T. Weber, Correlated local dipoles in PbTe, Phys. Rev. Mater. **2**, 085402 (2018).

[30] P. Fons, A. V. Kolobov, M. Krbal, J. Tominaga, K. S. Andrikopoulos, S. N. Yannopoulos, G. A. Voyiatzis, and T. Uruga, Phase transition in crystalline GeTe: Pitfalls of averaging effects, Phys. Rev. B **82**, 155209 (2010).

[31] B. Jalan, R. Engel-Herbert, N. J. Wright, and S. Stemmer, Growth of high-quality SrTiO$_3$ films using a hybrid molecular beam epitaxy approach, J. Vac. Sci. Technol. A **27**, 461 (2009).

[32] S. Salmani-Rezaie, L. Galletti, T. Schumann, R. Russell, H. Jeong, Y. Li, J. W. Harter, and S. Stemmer, Superconductivity in magnetically doped SrTiO$_3$, Appl. Phys. Lett. **118**, 202602 (2021).

[33] T. Schumann, L. Galletti, H. Jeong, K. Ahadi, W. M. Strickland, S. Salmani-Rezaie, and S. Stemmer, Possible signatures of mixed-parity superconductivity in doped polar SrTiO$_3$ films, Phys. Rev. B **101**, 100503(R) (2020).

[34] T. Q. Wang, K. Ganguly, P. Marshall, P. Xu, and B. Jalan, Critical thickness and strain relaxation in molecular beam epitaxy-grown SrTiO$_3$ films, Appl. Phys. Lett. **103**, 212904 (2013).

[35] See Supplemental Material at http://link.aps.org/supplemental/10.1103/PhysRevMaterials.5.104801 for x-ray diffraction data of films A–D, HAADF-STEM images of films A–D, additional analysis of nanodomains in different regions, and data on the superconductivity of the films shown in Fig. 4.

[36] J. M. LeBeau, S. D. Findlay, L. J. Allen, and S. Stemmer, Position averaged convergent beam electron diffraction: Theory and applications, Ultramicroscopy **110**, 118 (2010).

[37] H. Kim, J. Y. Zhang, S. Raghavan, and S. Stemmer, Direct Observation of Sr Vacancies in $SrTiO_3$ by Quantitative Scanning Transmission Electron Microscopy, Phys. Rev. X **6**, 041063 (2016).

[38] T. M. Bretz-Sullivan, A. Edelman, J. S. Jiang, A. Suslov, D. Graf, J. Zhang, G. Wang, C. Chang, J. E. Pearson, A. B. Martinson, P. B. Littlewood, and A. Bhattacharya, Superconductivity in the dilute single band limit in reduced strontium titanate, arXiv:1904.03121.

[39] A. D. Caviglia, M. Gabay, S. Gariglio, N. Reyren, C. Cancellieri, and J. M. Triscone, Tunable Rashba Spin-Orbit Interaction at Oxide Interfaces, Phys. Rev. Lett. **104**, 126803 (2010).

[40] K. Michaeli, A. C. Potter, and P. A. Lee, Superconducting and Ferromagnetic Phases in $SrTiO_3$/$LaAlO_3$ Oxide Interface Structures: Possibility of Finite Momentum Pairing, Phys. Rev. Lett. **108**, 117003 (2012).

[41] C. J. Liu, X. Yan, D. F. Jin, Y. Ma, H. W. Hsiao, Y. L. Lin, T. M. Bretz-Sullivan, X. J. Zhou, J. Pearson, B. Fisher, J. S. Jiang, W. Han, J. M. Zuo, J. G. Wen, D. D. Fong, J. R. Sun, H. Zhou, and A. Bhattacharya, Two-dimensional superconductivity and anisotropic transport at $KTaO_3$ (111) interfaces, Science **371**, 716 (2021).